Journal of Geophysical Research: Space Physics

RESEARCH ARTICLE
10.1002/2018JA025202

Special Section:
Mars Aeronomy

The Structure of Martian Magnetosphere at the Dayside Terminator Region as Observed on MAVEN Spacecraft

O. L. Vaisberg[1], V. N. Ermakov[1,2], S. D. Shuvalov[1], L. M. Zelenyi[1], J. Halekas[3], G. A. DiBraccio[4], J. McFadden[5], and E. M. Dubinin[6]

[1]Space Research Institute, Russian Academy of Sciences, Moscow, Russia, [2]National Research Nuclear University MEPhI, Moscow, Russia, [3]Department of Physics and Astronomy, University of Iowa, Iowa City, IA, USA, [4]NASA Goddard Space Flight Center, Greenbelt, MD, USA, [5]Space Sciences Laboratory, University of California, Berkeley, CA, USA, [6]Max Planck Institute for Solar System Research, Gottingen, Germany

Key Points:
- The dayside magnetosphere of Mars at ~70° SZA is a permanent domain of ~200 km thickness between the magnetosheath and the ionosphere
- Magnetopause is defined by a steep gradient of O^+ and O_2^+ densities, which increase by factor of 10^2–10^3 at interface with the ionosphere
- The structure of the dayside magnetosphere is controlled by directions of solar wind magnetic field and solar wind motional electric field

Correspondence to:
O. L. Vaisberg,
olegv@iki.rssi.ru

Citation:
Vaisberg, O. L., Ermakov, V. N., Shuvalov, S. D., Zelenyi, L. M., Halekas, J., DiBraccio, G. A., et al. (2018). The structure of Martian magnetosphere at the dayside terminator region as observed on MAVEN spacecraft. *Journal of Geophysical Research: Space Physics*, *123*. https://doi.org/10.1002/2018JA025202

Received 22 JAN 2018
Accepted 15 MAR 2018
Accepted article online 23 MAR 2018

Abstract We analyzed 44 passes of the Mars Atmosphere and Volatile EvolutioN mission (MAVEN) spacecraft through the magnetosphere, arranged by the angle between electric field vector and the projection of spacecraft position radius vector in the plane perpendicular to the Mars-Sun line (θ_E). All passes were divided into three angular sectors near 0°, 90°, and 180° θ_E angles in order to estimate the role of the interplanetary magnetic field direction in plasma and magnetic properties of dayside Martian magnetosphere. The time interval chosen was from 17 January to 4 February 2016 when MAVEN was crossing the dayside magnetosphere at solar zenith angle ~70°. Magnetosphere as the region with prevailing energetic planetary ions is always found between the magnetosheath and the ionosphere. The analysis of dayside interaction region showed that for each angular sector with different orientation of the solar wind electric field vector $\boldsymbol{E} = -1/c\ \boldsymbol{V} \times \boldsymbol{B}$ one can find specific profiles of the magnetosheath, the magnetic barrier (Michel, 1971, https://doi.org/10.1029/RG009i002p00427; Zhang et al., 1991, https://doi.org/10.1029/91JA00088), and the magnetosphere. Magnetic barrier forms in front of the magnetosphere, and relative magnetic field magnitudes in these two domains vary. The average height of the boundary with ionosphere is ~530 km, and the average height of the magnetopause is ~730 km. We discuss the implications of the observed magnetosphere structure to the planetary ions loss mechanism.

Plain Language Summary As Mars does not have an intrinsic global magnetic field, the solar wind directly interacts with the gaseous envelope of Mars. This interaction leads to formation of the magnetosphere from magnetic field tubes of the solar wind that bend around the planet forming magnetoplasma envelope around it. The dayside of the magnetosphere was not studied in detail due to its relatively small scale. MAVEN spacecraft with its comprehensive payload gives possibility for studying the dayside magnetosphere of Mars. Analysis of MAVEN plasma and magnetic measurements showed that the dayside Martian magnetosphere is a permanent layer of the magnetized plasma between heated solar wind plasma flow and the ionosphere. With average thickness of ~200 km it is filled with planetary ions accumulated during convection of these tubes from the dayside to the tail. These ions then escape through the tail being the one of the primary loss sources that led to devastating the Martian atmosphere through millennia. It is found that the magnetic structure and planetary ion flux in dayside magnetosphere are asymmetric to what is determined by the direction of the interplanetary magnetic field. This asymmetry is analyzed in the paper.

1. Introduction

The obstacle to the solar wind flow at Mars has been observed for more than 45 years by several spacecraft. First crossings of the dayside magnetosphere with observations of increasing magnetic field up to ~30 nT (Dolginov et al., 1972) and ions of lower energy than magnetosheath ions were made by Mars 2 and Mars 3 (called then "ion cushion"; Bogdanov & Vaisberg, 1975). The ion and magnetic tail at ~7 R_M with planetary ions outflow was found on Mars 5 (Dolginov, 1978; Vaisberg, 1976). The magnetic field increase, solar wind proton depression, and the presence of planetary ions were interpreted in terms of the boundary layer existence on the dayside (Szego et al., 1998).

Ion composition within the magnetic barrier at dayside of Mars was measured on Mars Express (Dubinin, Modolo, Fraenz, Woch, Chanteur, et al., 2008; Dubinin, Modolo, Fraenz, Woch, Duru, et al., 2008). The cases of strong mass loading and the magnetic field pileup with discontinuity (the magnetic pileup boundary)

were found as well as the crossings of the Martian magnetosphere on the dayside without a signature of a magnetic field pileup. The altitude of the magnetic barrier near subsolar point was 450–550 km independent on strong solar wind ram pressure variations. Rather sharp ionospheric photoelectron boundary with abruptly increasing photoelectron number density on this boundary up to ~$10^3/cm^{-3}$ was found.

Halekas et al. (2017) stated that "the magnetosphere of Mars forms as a result of the direct and indirect interaction of the solar wind with the Martian ionosphere, through a combination of induction effects and mass loading". The Martian magnetosphere is dominated by plasma of atmospheric origin, which forms the primary global obstacle to the solar wind through induction and mass loading, with additional contributions from localized crustal magnetic fields (Halekas et al., 2017).

Matsunaga et al. (2017) analyzed 10 months of Mars Atmosphere and Volatile EvolutioN mission (MAVEN) observations to determine the average locations of Ion Composition Boundary, Induced Magnetosphere Boundary, and Pressure Balance Boundary. They found that Induced Magnetosphere Boundary almost coincides with Ion Composition Boundary on the dayside.

Vaisberg et al. (2017) analyzed one case of Martian magnetosphere crossing by MAVEN spacecraft at terminator region, characterized by high mass loading. In this case the equality of magnetic and kinetic energies was observed, which means that the regime of magnetospheric plasma flow is Alfvenic.

The structure and properties of the dayside Martian magnetosphere are much less studied than the nightside of it due to its small-scale and insufficient temporal resolution of previous Martian satellites. These may be the reasons for misconceptions of Marian magnetosphere including its name as "induced magnetosphere" and the conclusion that the solar wind directly interacts with Martian ionosphere.

Mars Atmosphere and Volatile EvolutioN mission (MAVEN) with comprehensive high time resolution instruments suite provided an excellent possibility to study Martian environment. We analyze the structure and the properties of the dayside Martian magnetosphere near terminator in MSE coordinate system that shows the role of interplanetary magnetic field direction in plasma and the magnetic properties of the dayside Martian magnetosphere.

The plan of the paper is the following. An example of MAVEN dayside pass at Mars is given to discuss how the boundaries of magnetosphere are identified. Selected passes through the magnetosphere were divided in three sectors depending on θ_E coordinate system. The typical properties of the magnetic barrier and the magnetosphere in each sector are summarized and exemplified. The dependence of the lower and upper boundaries of magnetosphere in MSE coordinates is shown. The estimation of the heavy ion flux within the magnetosphere is given. The discussion of some magnetospheric properties is given.

2. Observations

We are using the data of the following MAVEN instruments: Suprathermal and Thermal Ion Composition (STATIC; McFadden et al., 2015), Solar Wind Ion Analyzer (SWIA; Halekas et al., 2015, 2017), and magnetometer (MAG; Connerney et al., 2015, 2015).

The Suprathermal and Thermal Ion Composition (STATIC) instrument is designed to measure the ion composition and distribution function of Martian ionosphere within 360° × 90° field of view (FOV). The energy range of the instrument is from 0.1 eV/e to 30 keV/e. Being equipped with a time-of-flight velocity analyzer, STATIC is capable of resolving the major ion species near Mars, including H^+, He^+, O^+, and O_2^+. In order to provide the capability of ram ions measurements, the instrument is mounted on the Articulated Payload Platform, a 2 m boom, which points its FOV into the ram direction at periapsis, leading to the frequent change of its orientation during the orbit.

The Solar Wind Ion Analyzer (SWIA) instrument, designed for measuring solar wind ions, provides ion velocity distributions with high energy resolution (14.5%) and angular resolution (3.75° × 4.5° in the sunward direction and 22.5° × 22.5° elsewhere) in 360° × 90° FOV. The instrument is mounted on the main deck of the spacecraft, and its orientation was chosen to maximize the coverage of the ion flow direction.

The magnetometer (MAG) directly measures the three components of magnetic field with 32-Hz cadence. In particular, we use these measurements to estimate the interplanetary magnetic field when the spacecraft is outside the bow shock, which is essential for calculating the upstream convection electric field.

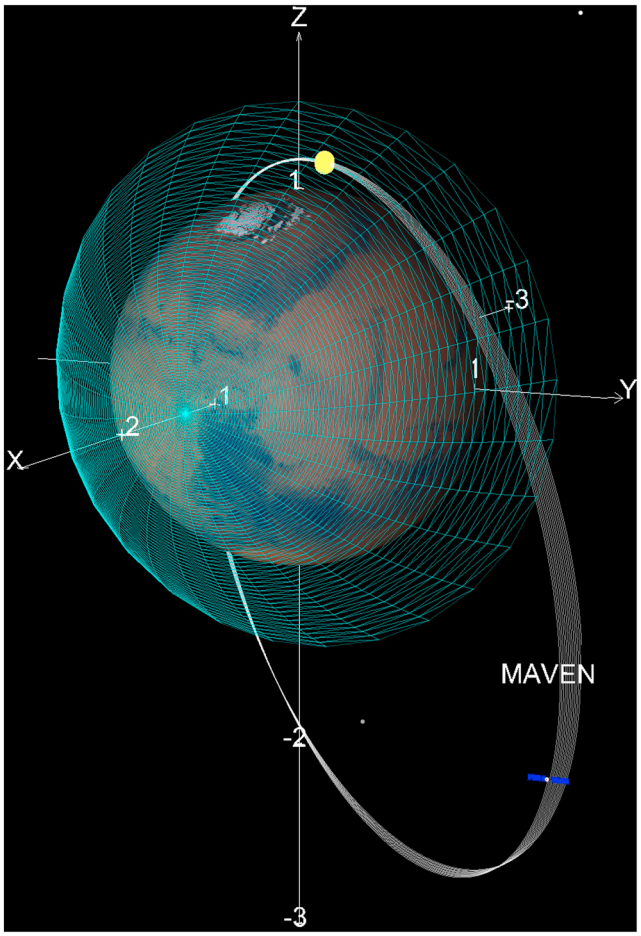

Figure 1. MAVEN orbits from 17 January to 4 February 2016 (from 3DView science tool for 3-D visualization, http://3dview.irap.omp.eu). Blue gridded surface shows magnetospheric pileup boundary (MPB) according to Edberg et al. (2008). Yellow dot shows the intersection of MAVEN with MPB.

The inward passes of MAVEN through dayside of solar wind-Mars interaction region were chosen in order to minimize the time interval between the pass of MAVEN from the solar wind to the magnetosphere. The time interval chosen was from 17 January to 4 February 2016 when MAVEN crossed the dayside magnetosphere at solar zenith angle (SZA) ~70° (Figure 1). This time interval was chosen such that crossings of dayside magnetosphere were in the northern hemisphere of Mars where the possible influence of magnetic anomalies is minimal. The flank region of magnetosphere was chosen for analysis so that it should be relatively far from the subsolar region where Martian magnetosphere is forming and relatively close to terminator that provides plasma for the nightside magnetosphere of Mars.

The passes of MAVEN within selected time interval were arranged according to the θ_E angle (the angle between electric field vector and the projection of spacecraft position radius vector in the *YZ* plane in MSE coordinate system) in MSE coordinate system with *X* axis directed to the Sun, *Z* axis directed along vector $\boldsymbol{X} \times \boldsymbol{B}_{\mathbf{SW}}$, and *Y* completing to the right system between the solar wind motional electric field vector $\boldsymbol{E} = -1/c\ \boldsymbol{V} \times \boldsymbol{B}$ direction. This coordinate system is also called the magnetic coordinate system (Figure 2). The solar wind electric field was computed from the table compiled by one of the co-authors (SWIA PI J. Halekas) from SWIA and MAG (J. Connerney PI) measurements.

We decided to analyze four sectors of the magnetosphere rather than all circle as these sectors are the ones with extreme locations in MSE coordinate system and, in the case of existing asymmetry, we can reveal it with higher probability.

We have chosen for analysis sectors in MSE coordinates with very different conditions rather than analyze all azimuths.

Altogether, 44 inbound passes were selected for analysis according to their positions in three angular intervals: #1, 0°–30° (18 crossings); #2, 60°–120° (14 crossings); and #3, 150°–180° (13 crossings).

There was no allowance for the sign of θ_E angle in this selection. The distribution of magnetosphere passes over the calculated MSE θ_E angles is shown in Figure 3.

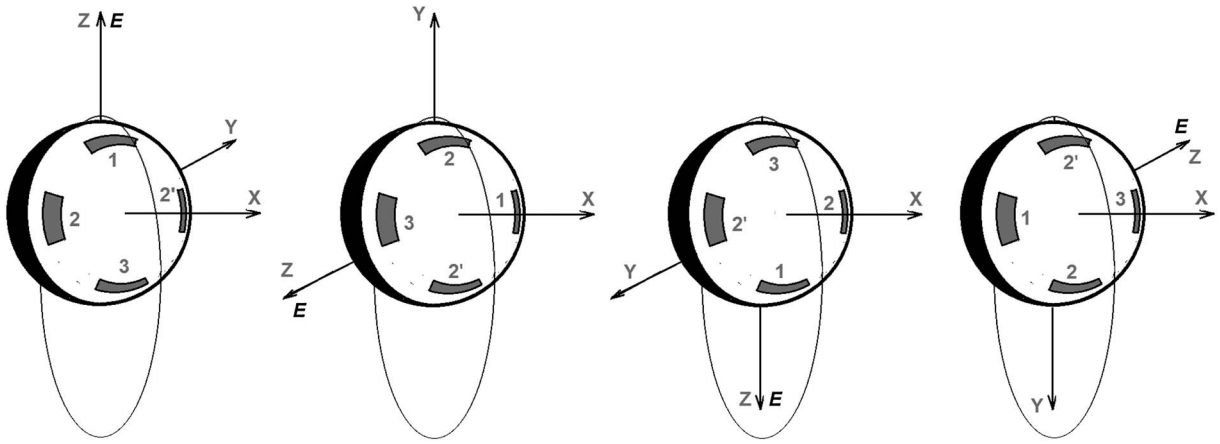

Figure 2. The angular sectors selected for analysis (shaded areas approximately show magnetospheric sectors) in MSE coordinate system. Sectors #2 and #2' shown in the picture are referred as sector #2 in text. From left to right: cases of MAVEN magnetospheric crossings in one of four sectors with angle θ_E between electric field *E* and the spacecraft approximate location during magnetosphere crossing: (a) $\theta_E = 0°$, (b) $\theta_E = 90°$, (c) $\theta_E = 180°$, and (d) $\theta_E = -90°$.

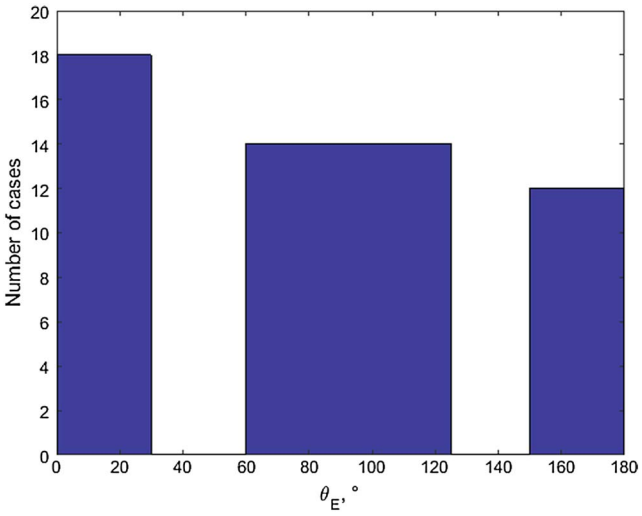

Figure 3. Distribution of passes through magnetosphere according to the θ_E angle in MSE coordinates. The height of each bar is the number within angular sector that is the width of the bar.

3. Analysis

3.1. An Example

Initial analysis was made with the use of quick looks plotted in AMDA database (science analysis system provided by the Centre de Données de la Physique des Plasmas supported by Centre national de la recherche scientifique, Centre national d'études spatiales, Observatoire de Paris, and Université Paul Sabatier, Toulouse, http://amda.cdpp.eu/) and quantitative plots with use of MatLab programs. Figure 4 shows the crossing of dayside solar wind-Mars interaction region from the group 1 (θ_E angle 13.35°). From left to right: the solar wind, the magnetosheath, the magnetosphere, and the ionosphere.

The bow shock was crossed at ~09:19 UT as seen by the magnetic field jump and ion deceleration and heating. The magnetosheath continues until protons number density decrease and oxygen ions density increases at ~09:43 UT. Noticeable oxygen ions are seen in the magnetosheath, and they can be seen as more energetic (~3 keV) component on STATIC and SWEA energy-time spectrograms (the plume—a beam of oxygen ions accelerated by the solar wind motional electric field; Andrews et al., 2016; Dong et al., 2015, 2017; Liemohn et al., 2014). The magnetic barrier (the steep monotonic rise of the magnetic field magnitude) was entered at ~09:32 UT. The magnetic barrier in front of planetary obstacle to the solar wind was considered as a possibility (Michel, 1971) and was observed for the first time at Venus by Zhang et al. (1991). The magnetosphere can be seen as oxygen-dominated region from magnetopause at ~09:43 UT till ionosphere at ~09:47:00 UT. Magnetic field in the magnetic barrier continues to rise with maximum of ~23 nT in the magnetosphere and then decreases to ~16 nT at the ionopause.

Figure 5 shows the properties of the plasma and the magnetic field in more detail. Numerical parameters allow us to determine the location of boundaries and identification of regions more precisely. The

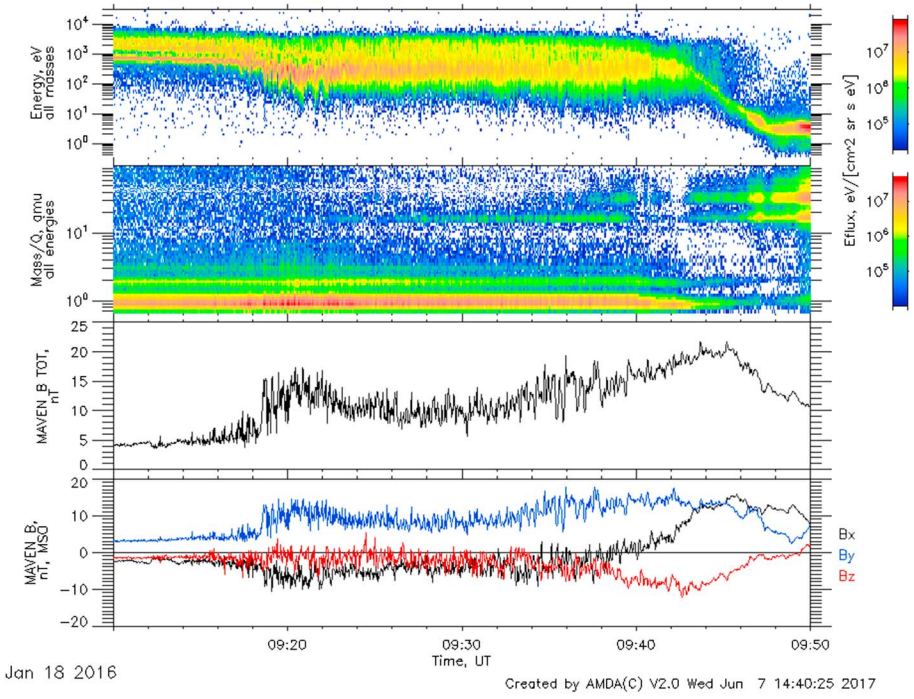

Figure 4. Overview of MAVEN inbound pass on 18 January 2016. From top to bottom: STATIC energy-time spectrogram (all ions), STATIC ion mass-time spectrogram, MAG magnetic field magnitude, and MAG magnetic field components. AMDA (http://amda.cdpp.eu/). θ_E angle is 13.35°.

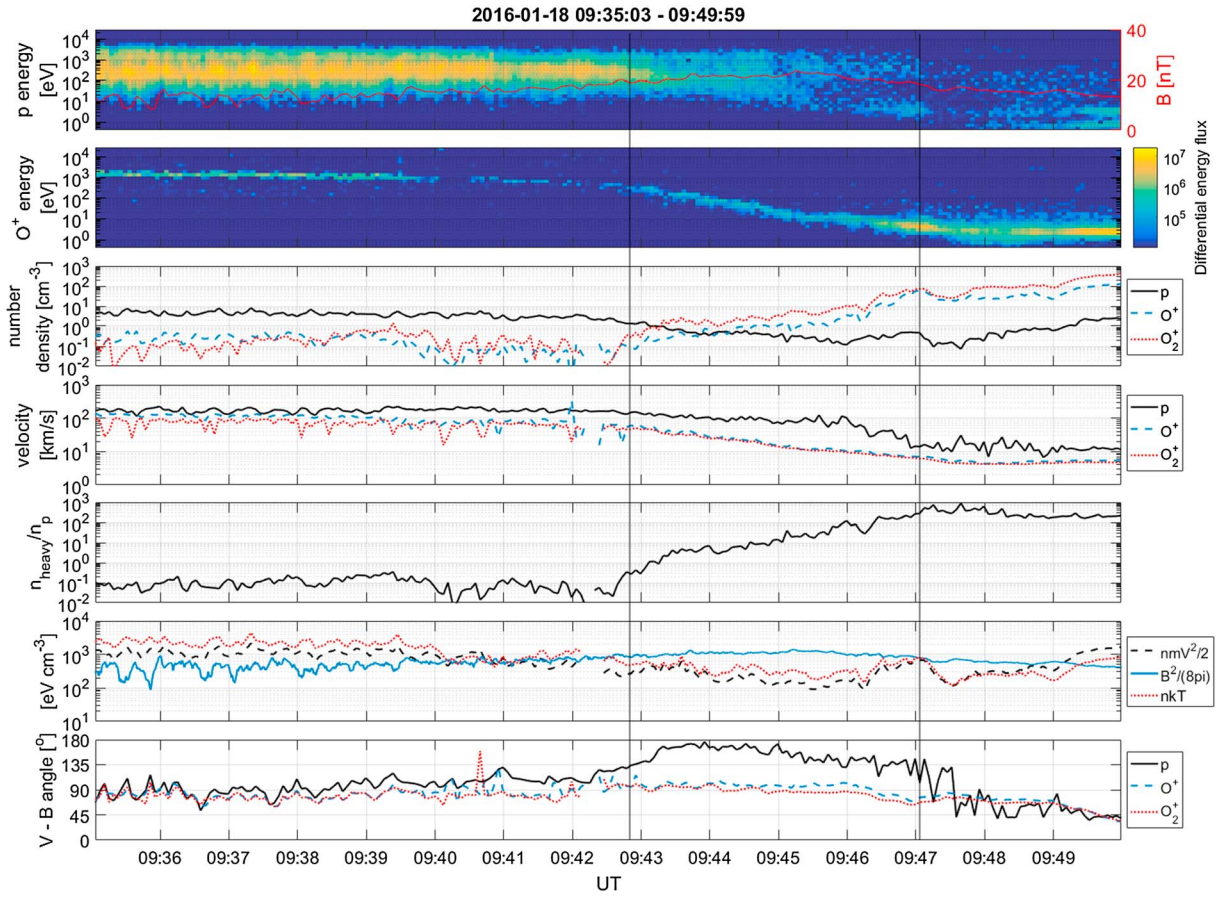

Figure 5. From top to bottom: the proton and O^+ energy-time spectrograms; the number densities of protons, O^+, and $O_2{}^+$ ions; the ratio of ($O^+ + O_2{}^+$) sum number density to proton number density; magnetic, kinetic, and thermal energy densities; and the angles between the magnetic field direction and the ions ram velocities. The vertical lines define the magnetospheric boundaries. θ_E angle is 13.35°.

magnetosheath is usually defined by the domination of plasma flow energy. However, the magnetic barrier brings some correction due to the increase of magnetic energy and leads to partial loss of protons and alpha particles. The approximate equality of the plasma and the magnetic pressure characterizes the Alfvenic flow.

The magnetosphere in the case shown is the region where the magnetic energy dominates. The heavy ions number density increases by more than 2 orders of magnitude from the magnetopause to the ionopause. The angle between the heavy ions velocity and the magnetic field direction is close to 90° that suggests an effective pickup. The proton component in the magnetosphere moves at the angle ~140°–180° to the magnetic field direction that facilitates the loss of protons along the field line. Indeed, the loss of more energetic protons is seen in the energy-time spectrogram upstream of the magnetopause.

Considering magnetosphere as the region between the magnetosheath flow of the solar wind plasma and the ionosphere, we determined outer magnetosphere boundary (magnetopause) by $n(O^+ + O_2{}^+)/n(p)$ ratio being in the range of 0.1 to 1 and/or its sharp increase in conjunction with proton energy drop. In most cases this boundary coincided with moderate increase of the magnetic field. Thus, the external boundary of the magnetosphere was similar to Ion Composition Boundary. It is worth noting that in the sector of 0°–30° θ_E angle the magnetosphere location was complicated by plume heavy ions, which could disturb the magnetosheath and magnetospheric flows.

In order to determine the magnetosphere-ionosphere boundary, we used the heavy ions energy-time spectrograms. This boundary was identified as a transition from wider energy component with higher average energy to more dense, steady low-energy and cold heavy ion components (ionosphere). For 0°–30° sector, mostly observed with plume, this boundary was identified as a transition from energy component with higher average energy to steady low-energy and cold heavy ions components (ionosphere).

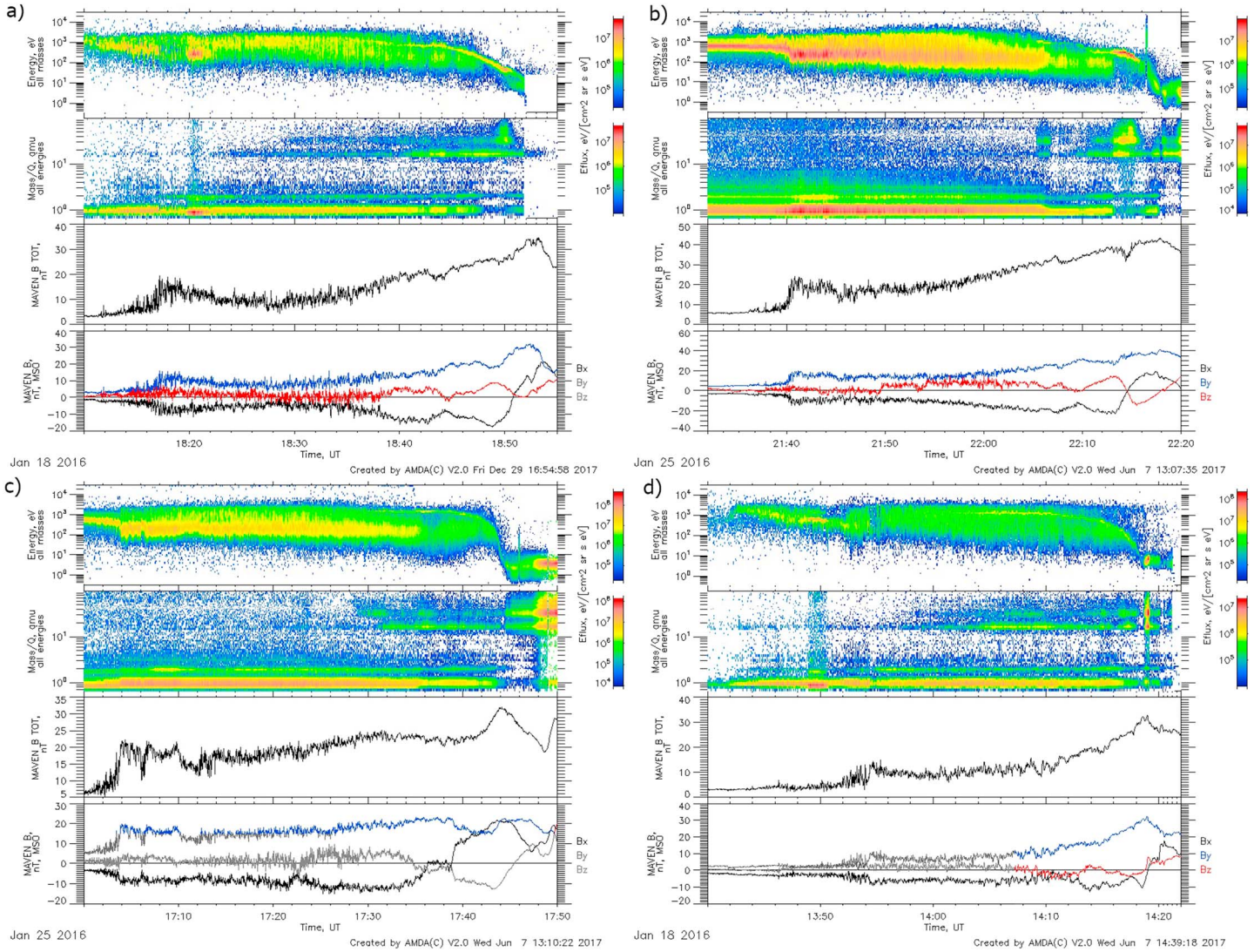

Figure 6. Four crossings of the magnetosphere at low θ_E angles (MSE sector #1). From top to bottom: energy-time spectrogram of all ions as measured by STATIC, the magnetic field magnitude, and the three components measured by MAG. θ_E angles are as follows: (a) 7.26°, (b) 23.11°, (c) −12.27°, and (d) −11.42°.

3.2. Sector 1: 0°–30°

Figures 6 and 7 show the typical magnetosphere crossings at high magnetic latitude, that is, at small θ_E angle in MSE coordinate system.

Most of the crossings at high MSE latitude have many similar properties. They are as follows:

1. Magnetosphere is always observed between the magnetosheath flow and ionosphere as a region dominated by planetary ions O^+ and $O_2{}^+$ with continuously decreasing velocity. The density of planetary ions increases by the factor of 10^2–10^3 from the magnetosheath to ionosphere.
2. Magnetopause as the outer boundary of magnetosphere is characterized by relatively sharp increase of $(n(O^+) + n(O_2{}^+))/n(p)$ ratio. In some cases heavy ions density at magnetopause is accompanied by the increase of magnetic field magnitude.
3. Magnetic barrier is found in all passes. It continues in magnetosphere with increasing magnitude. Maximum B is usually observed within magnetosphere or at the boundary between the magnetosphere and the ionosphere. In most cases magnetic field magnitude is smaller in the ionosphere than in the magnetosphere.

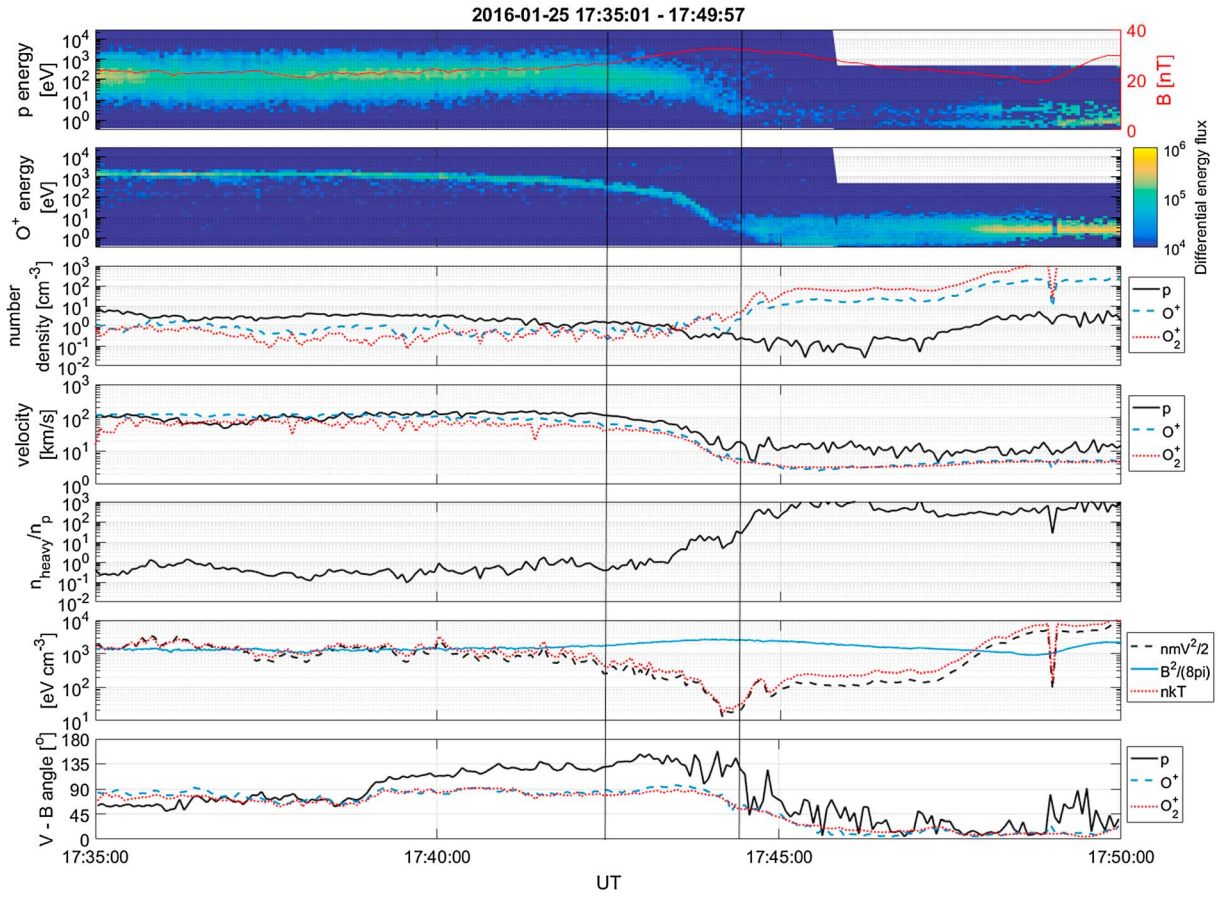

Figure 7. From top to bottom: proton and O^+ energy-time spectrograms; the number densities of protons, O^+, and $O_2{}^+$ ions; the ratio of ($O^+ + O_2{}^+$) number density to proton number density; magnetic, kinetic, and thermal energy densities; and the angles between the magnetic field direction and the ions ram velocities. The vertical lines define magnetospheric boundaries. Note the dominance of the magnetic energy in the magnetosphere and in the upper part of the ionosphere. θ_E angle is −12.27°.

4. Plume ions are seen in magnetosheath or magnetosphere or both. Strongest plume ion flux leads to the decrease of magnetic field magnitude in magnetic barrier in the magnetosphere.
5. Magnetic pressure dominates in the magnetosphere.
6. The density of magnetosheath protons decreases in the ionosheath/magnetic barrier layer adjacent to the magnetosphere. The density of protons strongly diminishes in the magnetosphere. The protons in the magnetosphere are moving at a relatively small angle to the magnetic field direction. The heavy ions move nearly perpendicular to the magnetic field direction.
7. The inner boundary of magnetosphere with ionosphere is difficult to locate due to existence of heated and accelerated ionospheric ions.

3.3. Sector 2: 60°–120°

The structures of the magnetosheath, the magnetic barrier, and the magnetosphere in this region of MSE are very variable Figure 8 shows four crossings of magnetosphere in this sector.

The properties of the magnetosphere and its surrounding in this region are the following:

1. Magnetic barrier and magnetosphere profiles are quite variable in this sector.
2. Magnetic barrier is frequently structured and may be less developed.
3. Magnetosheath proton flux is diluted in front of magnetosphere; density of higher-energy protons decreases.
4. Magnetic field magnitude has maximum in the magnetosphere.
5. There are cases of multiple crossings of the magnetopause.

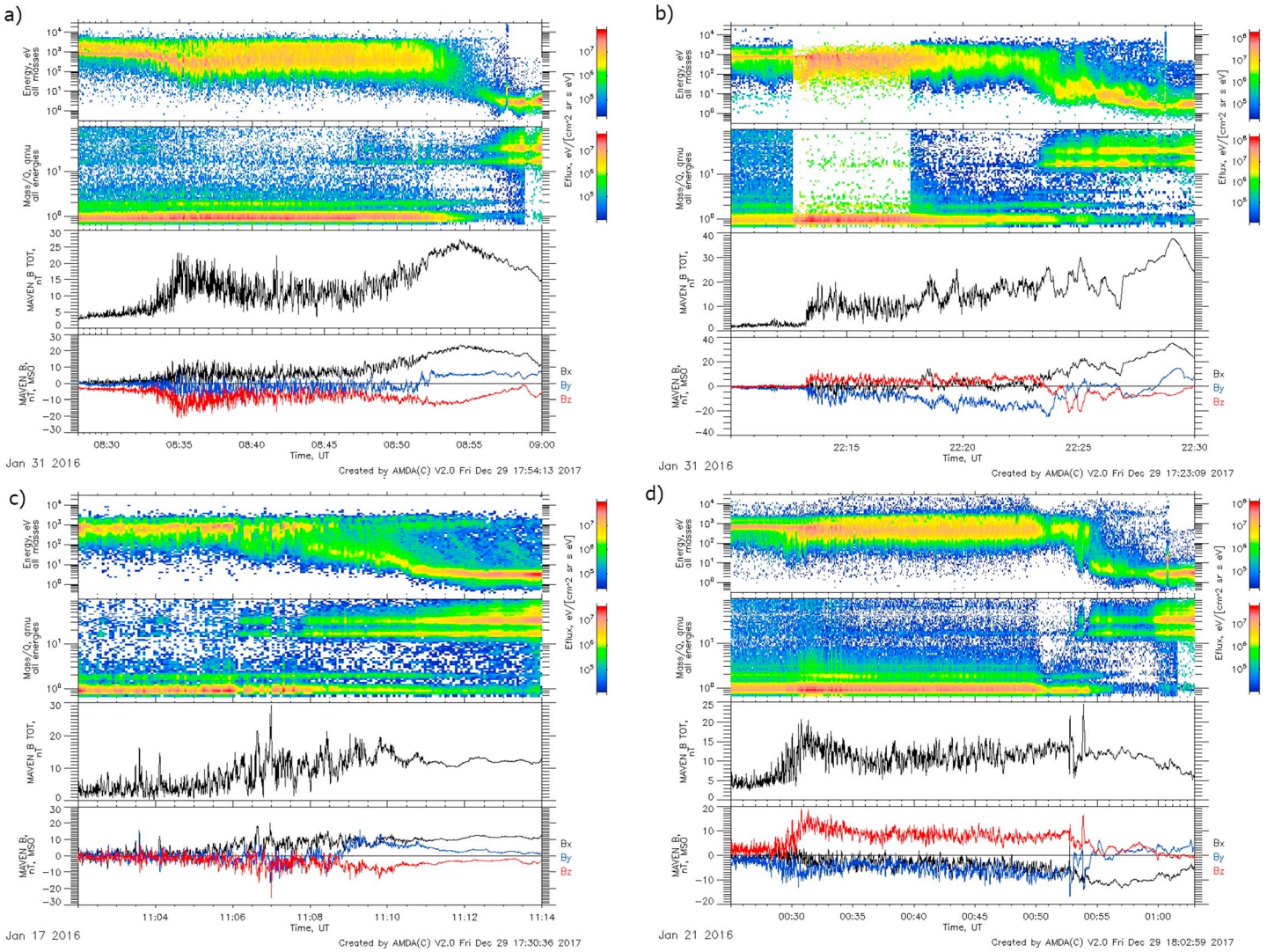

Figure 8. Four crossings of the magnetosphere at about 90° θ_E angles (MSE sector #2). From top to bottom: energy-time spectrogram of all ions as measured by STATIC, the magnetic field magnitude, and the three components measured by MAG. θ_E angles are as follows: (a) −122.79°, (b) −123.66°, (c) −62.07°, and (d) 106.92°.

6. The structure of plasma in magnetosphere is disturbed.
7. There are energy-dispersed signatures in the magnetosphere.

Figure 9 shows the properties of the plasma, the magnetic field, and the derived parameters for two crossings in more detail. The pass on 31 January 2016 at ~08:44–09:02 UT shows the well-ordered magnetosphere in which magnetic field pressure dominates. The pass on 31 January 2016 at ~22.21–09:02 UT shows very chaotic structure. Plasma and magnetic pressures are variable with changing ratio of magnitudes.

3.4. Sector 3: 160°–180°

Figure 10 shows four examples of MAVEN passes in 160°–180° MSE sector.

Most of the crossings at high MSE latitude have many similar properties. They are as follows:

1. Mass loading of magnetosheath is small and consists of O^+ ions.
2. Magnetic field in magnetic barrier is weak and quite thin.
3. The proton velocity in the magnetosheath is nearly constant till the magnetopause.
4. There is a region of smaller protons number density in front of the magnetosphere.
5. Magnetic field often has minimum at magnetopause.

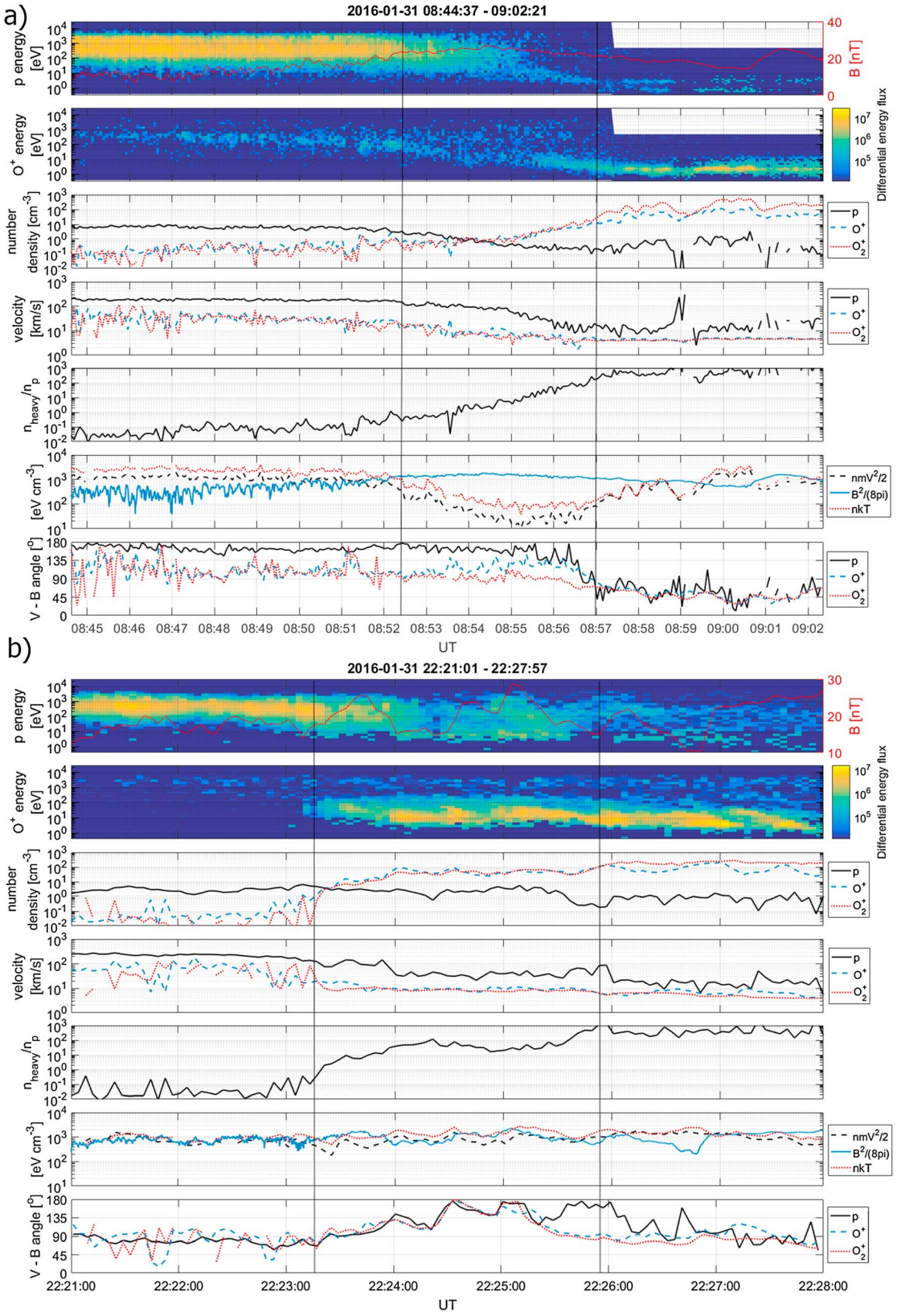

Figure 9. From top to bottom: proton and O^+ energy-time spectrograms; number densities of protons, O^+, and $O_2{}^+$ ions; the ratio of sum ($O^+ + O_2{}^+$) number density to proton number density; magnetic, kinetic, and thermal energy densities; and the angles between the magnetic field direction and the ions ram velocities. θ_E angles are as follows: (a) −122.79° and (b) −123.66°.

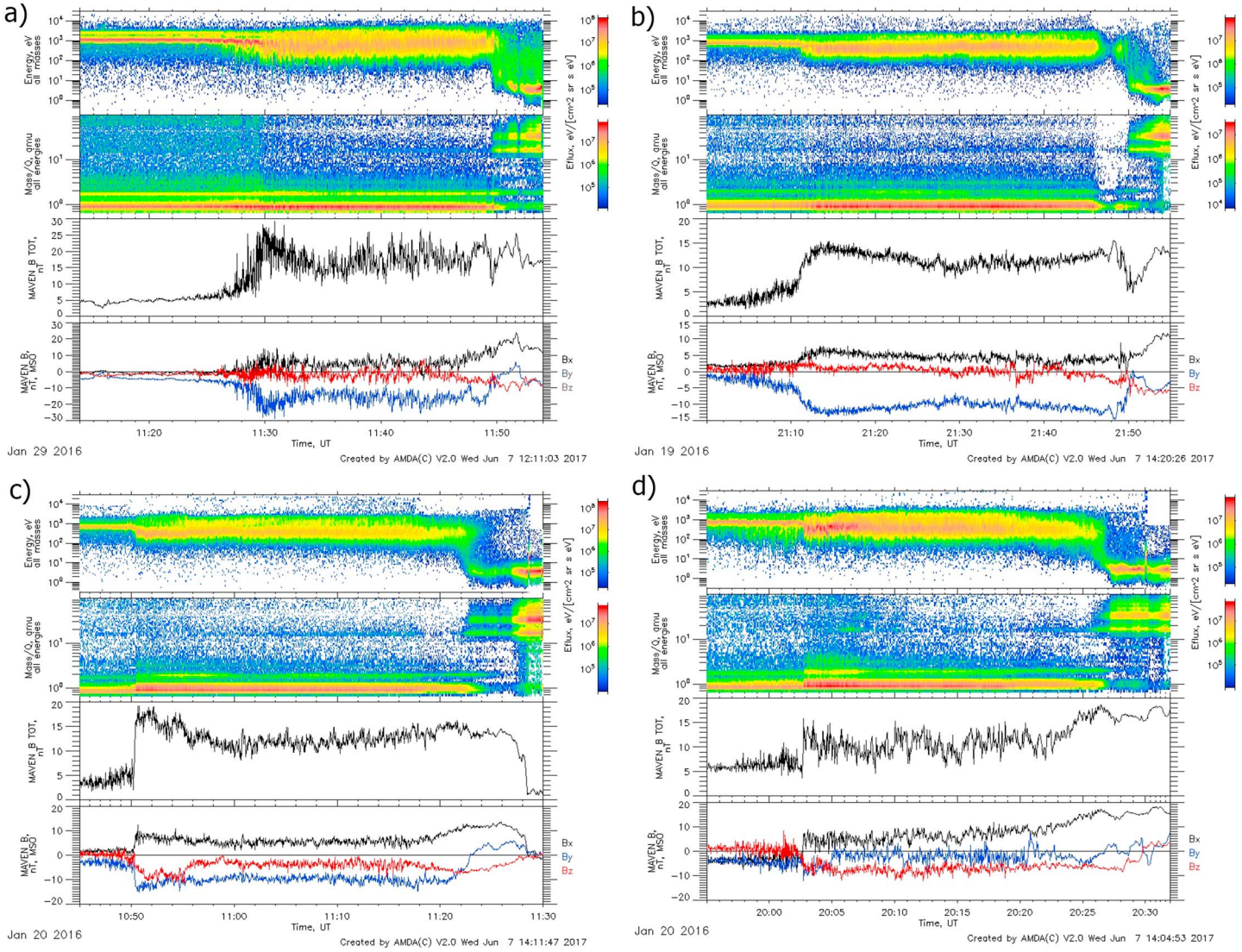

Figure 10. Four examples of MAVEN passes at 160°–180° θ_E angles (MSE sector #3). From top to bottom: energy-time spectrogram of all ions as measured by STATIC, the magnetic field magnitude, and the three components measured by MAG. θ_E angles are as follows: (a) −179.29°, (b) 167.53°, (c) −168.82°, and (d) −161.98°.

6. Density gradient of O^+ and O_2^+ ions at magnetopause is higher at magnetopause than in other sectors.
7. The magnetic field magnitude is sometimes smaller in the magnetosphere than in the adjacent magnetosheath.
8. Magnetospheric ions have relatively small energy and sometimes wide energy spectrum.
9. The thickness of the magnetosphere is small.

The two passes across the magnetosphere in the sector are shown in Figures 11a and 11b: on 20 January 2016 at ~02:20 UT and 21 January 2016 at ~23:28 UT. One can see that energy distributions are different in this θ_E sector.

3.5. Boundaries

The distributions of the lower boundary of the magnetosphere height and the magnetopause height in three magnetic latitude intervals are shown in Figure 12.

The heights of the boundaries determined as mentioned above and magnetosphere thicknesses are shown in Table 1. For the passes where authors were uncertain about the location of the boundaries, both the lower and upper estimations were accounted as separate measurements.

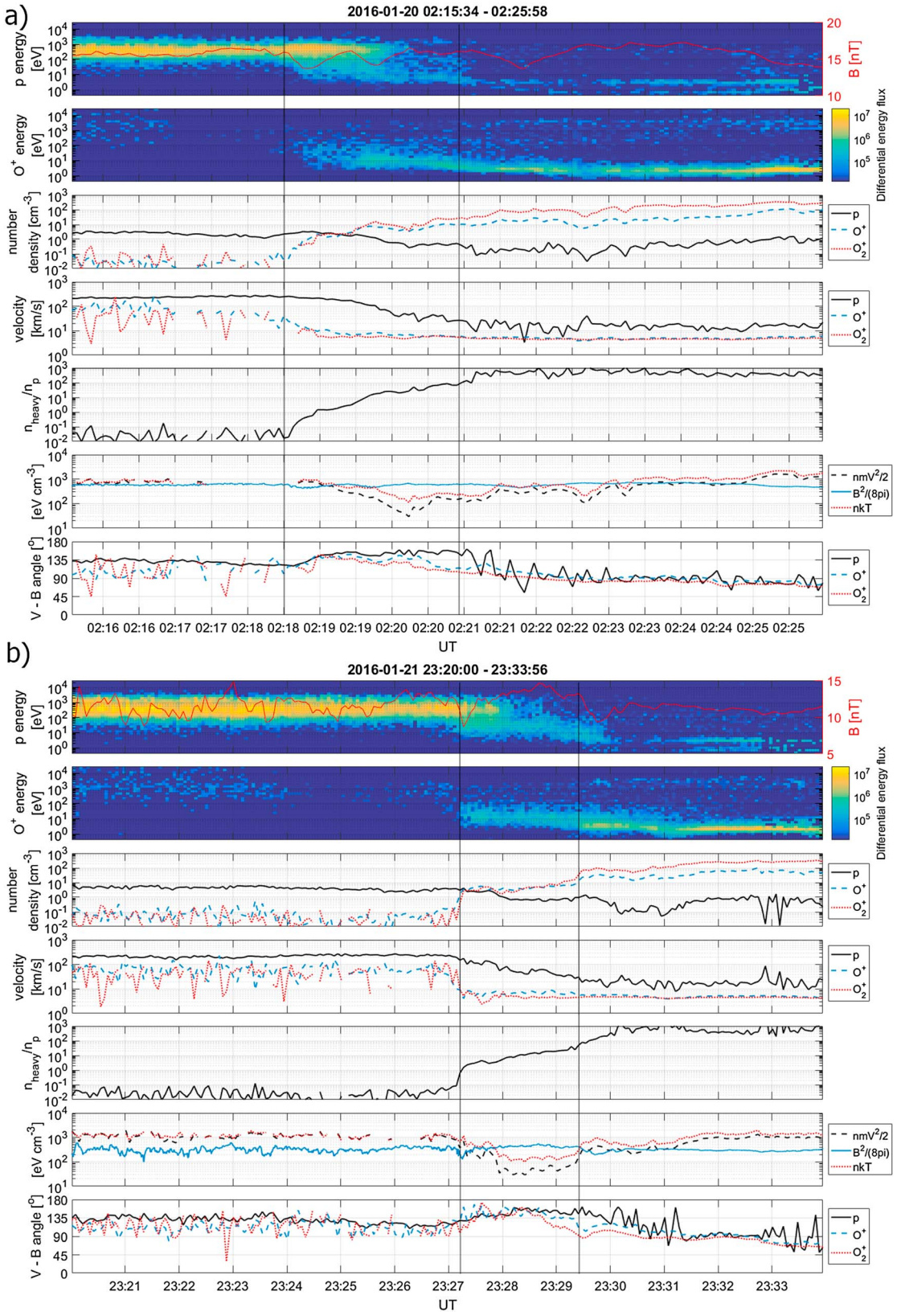

Figure 11. From top to bottom: proton and O^+ energy-time spectrograms; number densities of protons, O^+, and $O_2{}^+$ ions; the ratio of ($O^+ + O_2{}^+$) sum number density to proton number density; magnetic, kinetic, and thermal energy densities; and the angles between magnetic field direction and the ions ram velocities. θ_E angles are as follows: (a) −179.34° and (b) −165.54°.

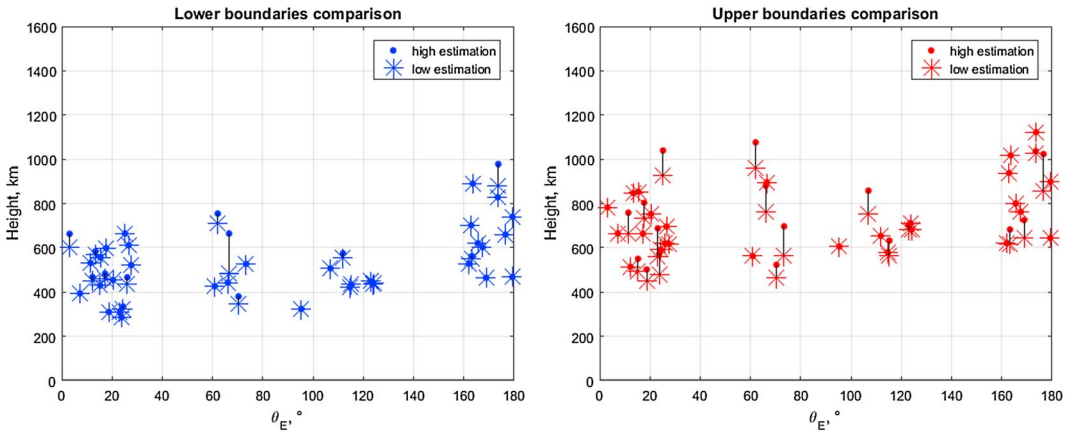

Figure 12. Height distributions of the magnetosphere boundaries in selected magnetic latitudes (MSE coordinates) intervals. (left) The boundary between the magnetosphere and the ionosphere and (right) the magnetopause.

3.6. Heavy Ions Flux

The approximate flux of heavy ions through the vertical cut of the magnetosphere with the width of 1 cm was calculated by the height integration of the measured flux along the trajectory of the spacecraft across the magnetosphere:

$$f_i = \int_{h_{\min}}^{h_{\max}} n_{b_i} v_{b_i} dh,$$

where i stands for the number of ion mass, f_i is the flux of this ion mass, n_b and v_b are the number density and the bulk velocity, respectively, h is the height, and $h_{\min}$ and $h_{\max}$ are the boundaries of the magnetosphere. The fluxes were calculated separately for three ions: p, O^+, and O_2^+ for each pass through the magnetosphere (Figure 13). As the field of view of STATIC frequently does not cover full sphere, each value needs to be considered as the lower value. The ion flux within sector #1 of the magnetosphere is often seen as a plume; its flux within the magnetosphere was included in the calculated flux. The median value of the calculated fluxes of heavy ions is about $f \sim 6 \times 10^{13}$ cm^{-1}/s. Multiplying this value by the length of the circle of the magnetosphere at SZA ~70° in allowing for the height of the magnetosphere $h \sim 600$ km, we receive the estimation of integral heavy ions flux f_{int} through the magnetospheric cross section $f_{\text{int}} = f \times 2\pi(R_M + h) \times \sin(70°) \sim 1.4 \times 10^{23}$/s. This is a lower value as STATIC field of view does not cover full sphere and part of the ion velocity distribution is not measured.

4. Discussion

All 44 MAVEN passes on Martian dayside at ~70° SZA angle considered in this paper showed the existence of the region between the magnetosheath flow and the ionosphere that we consider as the magnetosphere. In spite of the relatively small thickness, about 200 km at SZA ~70°, it plays important role in the formation of the nightside magnetosphere and the source of ions transported to the nightside and apparently lost through the tail. The properties of magnetosphere and its surrounding at SZA ~70° in three sectors of MSE coordinate system are presented in Table 2.

The majority of passes in sector #1 ($\theta_E \sim 0°$–$30°$) shows the plume (Andrews et al., 2016; Dong et al., 2015, 2017; Liemohn et al., 2014) within the magnetosphere and/or in the magnetosheath. At the same time, the

Table 1
Magnetosphere Boundary Heights and Magnetosphere Thickness at Different MSE Latitudes

Sector	Magnetopause height (km)	Magnetosphere-ionosphere boundary height (km)	Magnetosphere thickness (km)
0°–30°	673 ± 30	479 ± 23	200 ± 16
60°–120°	705 ± 34	493 ± 28	223 ± 22
160°–180°	838 ± 43	661 ± 45	183 ± 17

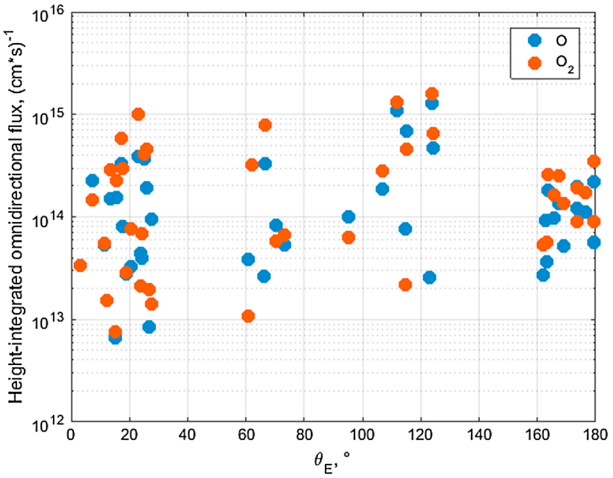

Figure 13. The calculated values of flux densities through 1-cm vertical cut of the magnetosphere.

density of the heavy ions in the magnetosphere is quite low when the magnetic pressure is high and plume is observed. The magnetic field magnitude usually has maximum within the magnetosphere in this MSE sector of magnetosphere. The strongest flux of the plume ions within the magnetosphere is accompanied by the magnetic field depression.

Figure 14 shows the pass of MAVEN on 19 January 2016 with the calculated directions of the electric field and the velocities of the heavy ions and protons. It is seen that the heavy ions are accelerated within the magnetosphere and produce the plume in the magnetosheath. This shows a significant fraction of the magnetospheric ions, which are accelerated to form the plume, thus leading to depletion of the magnetospheric ions. Consequently, the plume ions flux needs to be included to the flux of the magnetospheric ions in order to make a correct estimation of the total magnetospheric ion flux in sector #1.

The magnetic barrier in magnetic sector #1 of the magnetosphere develops in the magnetosheath and continues into the magnetosphere.

Table 2
The Properties of Magnetosphere and Its Surrounding at SZA ~70° in Three Sectors of MSE Coordinate System

	Sector 0°–30°	Sector 60°–120°	Sector 160°–180°
Magnetic barrier	Magnetic barrier is found in all passes. It continues in magnetosphere with increasing magnitude. In most cases magnetic field magnitude is smaller in the ionosphere than in the magnetosphere.	Magnetic barrier is frequently structured and may be less developed.	Magnetic field in magnetic barrier is weak. Magnetic barrier is relatively thin. Mass loading of magnetosheath is small and consists of O^+ ions.
Plume	Plume ions are seen in magnetosheath or magnetosphere or both. Strongest plume ion flux leads to decrease of magnetic field magnitude in magnetic barrier in magnetosphere.	Almost all passes do not show plume signatures.	None
Magnetosheath-magnetosphere interface	The density of magnetosheath protons decreases in the magnetosheath/magnetic barrier layer adjacent to the magnetosphere. The direction of proton velocity in the magnetosphere is sufficiently parallel to the magnetic field direction. The heavy ions move nearly perpendicular to the magnetic field direction.	Magnetosheath proton flux is diluted in front of magnetosphere. Higher-energy protons usually diminish faster.	Velocity of magnetosheath protons does not diminish at the magnetopause. Density of magnetosheath protons usually diminish in layer adjacent to magnetopause.
Magnetopause	Magnetopause as the outer boundary of magnetosphere is characterized by relatively sharp increase of (N_{O}^+ and N_{O2}^+)/N_p ratio. In some cases heavy ions density at magnetopause is accompanied by the increase of magnetic field magnitude.	Multiple crossings are frequent.	Magnetic field often has minimum at magnetopause. Density gradient of O^+ and O_2^+ ions at magnetopause is higher at the magnetopause than in other sectors.
Magnetic field maximum location	It is usually observed within the magnetosphere or at the boundary between the magnetosphere and the ionosphere.	Magnetic field has maximum in the magnetosphere.	Location of maximum *B* varies between magnetic barrier, magnetosphere, and ionosphere.
Magnetosphere	The density of protons strongly diminishes in the magnetosphere. The number densities of O^+ and O_2^+ ions increase from magnetopause to the interface with ionosphere by the factor of 10^2–10^3. Plume ions frequently dominate. The protons in the magnetosphere are moving at a relatively small angle to the magnetic field direction. The heavy ions move nearly perpendicular to the magnetic field direction.	The structure of plasma in magnetosphere is disturbed. There are energy-dispersed signatures in the magnetosphere.	Magnetospheric ions have relatively small energy and usually wide energy spectrum.
Interface with ionosphere	The inner boundary of magnetosphere with ionosphere is determined with smaller confidence due to diffuse nature of transition of the heavy ions energy between magnetosphere and ionosphere.		

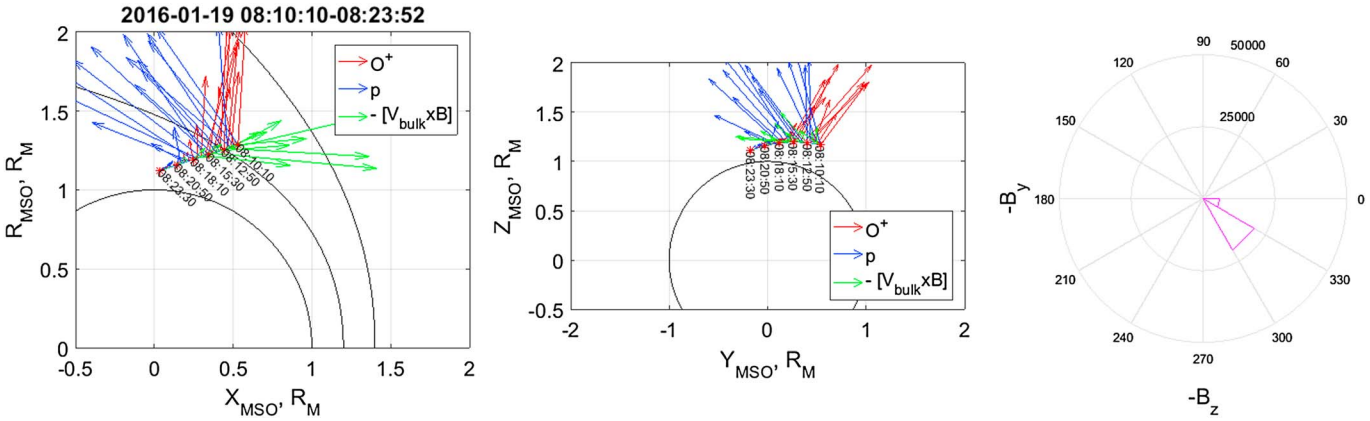

Figure 14. Electric field vectors (green), velocities of protons (blue), and O^+ ions (red) (left) in cylindrical coordinates X, $(X^2 + Z^2)^{1/2}$, (middle) in YZ_{MSO} plane, and (right) magnetosheath magnetic vectors distribution on B_y-B_z plane.

A large-scale rotation of the magnetic field frequently accompanies this transition. However, it is difficult to identify the magnetic pileup boundary in passes within this MSE sector and, consequently, to make a conclusion that the magnetic pileup boundary exists and whether plasma and magnetic boundaries coincide or not.

Sector #2 in MSE coordinate system (θ_E ~ 60°–120°) shows a large variety of the magnetospheric structures, and the ion flux and the magnetic field are variable along the spacecraft path. Like in sector #1, one can often see the depletion of more energetic protons in the part of the magnetosheath adjacent to the magnetopause and within the magnetosphere. The magnetospheric flow may be in Alfvenic regime, or the magnetic pressure can be higher than the plasma pressure. One can see multiple crossings of the magnetopause. These properties of the magnetospheric boundary in this sector suggest that either it is unstable or the mass loaded magnetic flux tubes are added to the magnetosphere in nonstationary regime.

The structure of the magnetosheath and the magnetic barrier in sector #3 in MSE coordinate system (θ_E ~ 160°–180°) is different from other sectors. There is no depletion of more energetic protons in front of the magnetopause. However, the density of the protons drops in the magnetic barrier that is consistent with the higher magnetic field magnitude than the one in the magnetosheath. The magnetosphere thickness is smaller than in other sectors of the magnetosphere, and it is located higher than the one in other sectors.

In sector #1 the average maximum of the magnetic field in the magnetosheath-ionosphere interface region is about 25–30 nT and is higher than in sector #3 where it is about 15–20 nT. In other words, the magnetic barrier in sector #1 is stronger than in sector #3. This can be associated with higher mass loading in sector #1 by the planetary plume ions ejected from the interface region by the motional electric field.

It is interesting to compare the heights of magnetospheric boundaries with other boundaries found in near-Mars space. Duru et al. (2009) found steep gradient of electron density at about 660 km at SZA 60°–70°. The SZA range is about the same for the observations in this paper. Withers et al. (2016) found photoelectron boundary median height of 620 km and magnetic pileup boundary median height of 970 km. The average location of the photoelectron boundary found by Garnier et al. (2017) at SZA ~70° is about 600 km. Our results can be compared with the electron boundary locations of Duru et al. (2009) and Garnier et al. (2017), both obtained at SZA favorably corresponding to the location of the observations used in this paper. The average height of the boundary between the ionosphere and the magnetosphere is 530 km. Thus, we can conclude that this boundary is most probably the planetary electron boundary.

The magnetic field magnitude frequently has the maximum within the magnetosphere and decreases toward the ionosphere. It means that the pressure balance on the dayside is not provided by the ionospheric current. This makes the term "induced magnetosphere" not well justified. This term was proposed in the earlier years of Mars and Venus investigations, mostly based on theoretical considerations. The model of Venusian magnetosphere (Vaisberg & Zelenyi, 1984; Zelenyi & Vaisberg, 1985) based on experimental data and analysis of the dayside Martian magnetosphere crossing (Vaisberg et al., 2017) gives evidence that the

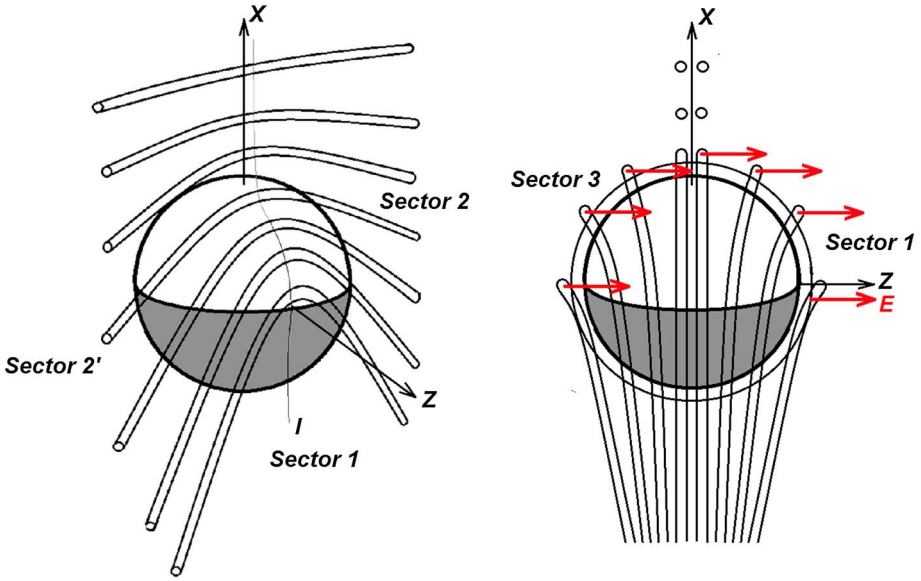

Figure 15. Two cartoons that schematically show the drift of the mass-loaded magnetic flux tubes within Martian magnetosphere. (left) Flux tubes move antiparallel to *X* axis until they enter magnetosphere near the subsolar point. Then they move around the planet while maximum mass loading leads to strong bending (line *l*). (right) View at *XZ* plane. Sector 1 is to the right, and sector 3 is to the left.

dayside magnetosphere is formed by the solar wind magnetic flux tubes entering the magnetosphere near the subsolar region and loaded by the planetary photoions during tubes' convection within the dayside magnetosphere to the terminator and then into the tail. In essence, this is mass-loaded magnetosphere or accretion magnetosphere.

Figure 15 shows schematically the way how the magnetosphere forms according to the model (Vaisberg & Zelenyi, 1984; Zelenyi & Vaisberg, 1985) and analysis performed in this paper. Current analysis emphasizes the importance of two main factors bringing about the significant asymmetry of the magnetosphere: (1) the angle between the axes of magnetic flux tubes and the direction of their convection through Martian dayside and (2) the direction of the solar wind electric field. In sectors #1 and #3 the convecting magnetic flux tubes accumulate photoions, and they predominantly rotate perpendicular to the direction of the magnetic field, so the mass loading continues steadily along the drift path. In sector #2 the solar wind pressure gradient effectively forces the solar wind protons (Zwan & Wolf, 1976) and, probably, the pickup ions to escape along the field line, predominantly more energetic ions (this mechanism works also in the magnetic barrier). The solar wind electric field plays an important role in providing the difference between sectors #1 and #3. The photoions mass loading the flux tubes during convection from the subsolar region to the terminator are subject to the solar wind electric field. However, while the solar wind electric field within the flux tubes in sector #1 accelerates and ejects ions from the magnetosphere into the magnetosheath producing the plume, the heavy ions accumulated in the magnetic flux tubes in sector #3 convect to the lower layer of the magnetosphere. While we see plume ions in sector #1 in magnetosheath, the pickup ions in sector #3 are cut at the magnetopause. The details of this process are outside the scope of this paper.

Using the value of median heavy ion flux through vertical column of magnetosphere $f \sim 6 \times 10^{13}$ cm^{-1}/s (see section 3.6) and dividing it by average thickness of magnetosphere ~200 km (see section 3.5), we receive the estimated median value of planetary ions (O^+ and O_2^+) flux density ~3×10^6 cm^{-2}/s at SZA ~70°. The flux density should increase during the convection of the magnetic flux tubes to the terminator and then to the tail. The average flux of O^+ ions in the boundary layer in the Martian tail is ~2×10^5 cm^{-2}/s (based on Dubinin et al., 2017), to which magnetospheric flow is the source. As the width of the boundary layer in the tail is larger than the thickness of the dayside magnetosphere, and the calculated heavy ions flux in the dayside magnetosphere includes two ion species, we can conclude that these two numbers are not contradictory.

5. Conclusion

The magnetosphere as specific domain between the magnetosheath flow and the ionosphere was identified in all 44 crossings of the dayside interaction region of the solar wind plasma with the Martian atmosphere at the solar zenith angle of ~70° in the northern part of the planet. The magnetopause is characterized by the stepwise increase of the number densities of the planetary ions O^+ and O_2^+ to protons ratio. The number densities of O^+ and O_2^+ ions increase by 2–3 orders of magnitude across the thickness of the magnetosphere, which is ~200 km on average. The energy of heavy ions decreases with the decrease of the altitude until it approximately equalizes to the energy of the ionospheric ions at the interface with the ionosphere. The number densities of the planetary ions and their height profiles indicate their origin as the pickup ions inside the magnetosphere. The magnetic flux tubes enter the magnetosphere in the subsolar region and accumulate the photoions on their convection to the terminator.

The structure of the magnetic barrier and the magnetosphere significantly varies with the location in MSE coordinates that is defined by the magnetic field direction and motional electric field direction. There are varieties in typical magnetosheath and magnetic barrier structures observed in different sectors of MSE coordinate system. In sector #1 magnetic barrier starts to form in the magnetosheath well outside the magnetosphere and the average maximum of the magnetic field magnitude reaches the values of 25–30 nT, which are higher than at other magnetic latitudes; in sector #2 magnetic barrier is frequently quite structured and may be less developed; in sector #3 magnetic barrier starts to form in the magnetosheath and the average maximum of the magnetic field magnitude reaches the values of 15–20 nT, which are lower than in sector #1.

The structure of the magnetospheric regions is determined by two main factors: direction of the interplanetary magnetic field and direction of the solar wind electric field. They control the ion pickup by the solar wind magnetic flux tubes entering the subsolar region of the magnetosphere, planetary photoions pickup and acceleration during flux tubes convection to terminator, acceleration and ejection of pickup ions with formation of the plume in the sector upward solar wind electric field, and pickup planetary ions confinement within the magnetosphere in opposite sector. In sector #2 the magnetosphere is quite disturbed that may be associated with nonsteady entry of the magnetic flux tubes in the magnetosphere.

Acknowledgments
The MAVEN project is supported by NASA through the Mars Exploration Program. MAVEN data are publicly available through the Planetary Data System. Authors O. V., L. Z., V. E., and S. S. wish to acknowledge support from the Russian Science Foundation by grant 16-42-01103. Author E. D. wishes to acknowledge DFG for supporting this work by grant PA 525/14-1 and support from DLR by grant 50QM1703. The authors are grateful to the team of the Centre de Données de la Physique des Plasmas (CDPP) for giving access to experimental data with the use of the AMDA data processing system, whose development was supported by CNRS, CNES, Observatoire de Paris, and Université Paul Sabatier, Toulouse.

References

Andrews, D. J., Barabash, S., Edberg, N. J. T., Gurnett, D. A., Hall, B. E. S., Holmström, M., et al. (2016). Plasma observations during the Mars atmospheric "plume" event of March–April 2012. *Journal of Geophysical Research: Space Physics*, *121*, 3139–3154. https://doi.org/10.1002/2015JA022023

Bogdanov, A. V., & Vaisberg, O. L. (1975). Structure and variations of solar wind-Mars interaction region. *Journal of Geophysical Research*, *80*(4), 487–494. https://doi.org/10.1029/JA080i004p00487

Connerney, J. E. P., Espley, J. R., Di Braccio, G. A., Gruesbeck, J. R., Oliversen, R. J., Mitchell, D. L., et al. (2015). First results of the MAVEN magnetic field investigation. *Geophysical Research Letters*, *42*, 8819–8827. https://doi.org/10.1002/2015GL065366

Connerney, J. E. P., Espley, J. R., Lawton, P., Murphy, S., Odom, J., Oliversen, R., & Sheppard, D. (2015). The MAVEN magnetic field investigation. *Space Science Reviews*, *195*(1-4), 257–291. https://doi.org/10.1007/s11214-015-0169-4

Dolginov, S. S. (1978). On the magnetic field of Mars: Mars 2 and Mars 3 evidence. *Geophysical Research Letters*, *5*(1), 89–92. https://doi.org/10.1029/GL005i001p00089

Dolginov, S. S., Yeroshenko, Y. G., & Zhuzgov, L. N. (1972). Magnetic field in the very close neighborhood of Mars according to data from the Mars-2 and Mars-3 spacecraft. *Doklady Akademii Nauk SSSR*, *207*(6), 1296.

Dong, Y., Fang, X., Brain, D. A., McFadden, J. P., Halekas, J. S., Connerney, J. E., et al. (2015). Strong plume fluxes at Mars observed by MAVEN: An important planetary ion escape channel. *Geophysical Research Letters*, *42*, 8942–8950. https://doi.org/10.1002/2015GL065346

Dong, Y., Fang, X., Brain, D. A., McFadden, J. P., Halekas, J. S., Connerney, J. E. P., et al. (2017). Seasonal variability of Martian ion escape through the plume and tail from MAVEN observations. *Journal of Geophysical Research: Space Physics*, *122*, 4009–4022. https://doi.org/10.1002/2016JA023517

Dubinin, E., Modolo, R., Fraenz, M., Woch, J., Chanteur, G., Duru, F., et al. (2008). Plasma environment of Mars as observed by simultaneous MEX-ASPERA-3 and MEX-MARSIS observations. *Journal of Geophysical Research*, *113*, A10217. https://doi.org/10.1029/2008JA013355

Dubinin, E., Modolo, R., Fraenz, M., Woch, J., Duru, F., Akalin, F., et al. (2008). Structure and dynamics of the solar wind/ionosphere interface on Mars: MEX-ASPERA-3 and MEX-MARSIS observations. *Geophysical Research Letters*, *35*, L11103. https://doi.org/10.1029/2008GL033730

Dubinin, E., Fraenz, M., Pätzold, M., McFadden, J., Halekas, J. S., DiBraccio, G. A., et al. (2017). The effect of solar wind variations on the escape of oxygen ions from Mars through different channels: MAVEN observations. *Journal of Geophysical Research: Space Physics*, *122*, 11,285–11,301. https://doi.org/10.1002/2017JA024741

Duru, F., Gurnett, D. A., Frahm, R. A., Winningham, J. D., Morgan, D. D., & Howes, G. G. (2009). Steep transient density gradients in the Martian ionosphere similar to the ionopause at Venus. *Journal of Geophysical Research*, *114*, A12310. https://doi.org/10.1029/2009JA014711

Edberg, N. J. T., Lester, M., Cowley, S. W. H., & Eriksson, A. I. (2008). Statistical analysis of the location of the Martian magnetic pileup boundary and bow shock and the influence of crustal magnetic fields. *Journal of Geophysical Research*, *113*, A08206. https://doi.org/10.1029/2008JA013096

Garnier, P., Steckiewicz, M., Mazelle, C., Xu, S., Mitchell, D., Holmberg, M. K. G., et al. (2017). The Martian photoelectron boundary as seen by MAVEN. *Journal of Geophysical Research: Space Physics*, *122*, 10,472–10,485. https://doi.org/10.1002/2017JA024497

Halekas, J. S., Brain, D. A., Luhmann, J. G., Di Braccio, et al. (2017). Flows, fields, and forces in the Mars-solar wind interaction. *Journal of Geophysical Research: Space Physics*, *122*, 11,320–11,341. https://doi.org/10.1002/2017JA024772

Halekas, J. S., Ruhunusiri, S., Harada, Y., Collinson, G., Mitchell, D. L., Mazelle, C., et al. (2017). Structure, dynamics, and seasonal variability of the Mars-solar wind interaction: MAVEN solar wind ion analyzer in-flight performance and science results. *Journal of Geophysical Research: Space Physics*, *122*, 547–578. https://doi.org/10.1002/2016JA023167

Halekas, J. S., Taylor, E. R., Dalton, G., Johnson, G., Curtis, D. W., McFadden, J. P., et al. (2015). The solar wind ion analyzer for MAVEN. *Space Science Reviews*, *195*(1-4), 125–151. https://doi.org/10.1007/s11214-013-0029-z

Liemohn, M. W., Johnson, B. C., Fränz, M., & Barabash, S. (2014). Mars Express observations of high altitude planetary ion beams and their relation to the "energetic plume" loss channel. *Journal of Geophysical Research: Space Physics*, *119*, 9702–9713. https://doi.org/10.1002/2014JA019994

Matsunaga, K., Seki, K., Brain, D. A., Hara, T., Masunaga, K., Mcfadden, J. P., et al. (2017). Statistical study of relations between the induced magnetosphere, ion composition, and pressure balance boundaries around Mars based on MAVEN observations. *Journal of Geophysical Research: Space Physics*, *122*, 9723–9737. https://doi.org/10.1002/2017JA024217

McFadden, J. P., Kortmann, O., Curtis, D., Dalton, G., Johnson, G., Abiad, R., et al. (2015). MAVEN SupraThermal and Thermal Ion Composition (STATIC) instrument. *Space Science Reviews*, *195*(1-4), 199–256. https://doi.org/10.1007/s11214-015-0175-6

Michel, F. C. (1971). Solar wind interaction with planetary atmospheres. *Review of Geophysics*, *9*(2), 427–435. https://doi.org/10.1029/RG009i002p00427

Szego, K., Klimov, S., Kotova, G. A., Livi, S., Rosenbauer, H., Skalsky, A., & Verigin, M. I. (1998). On the dayside region between the shocked solar wind and the ionosphere of Mars. *Journal of Geophysical Research*, *103*(A5), 9101–9111. https://doi.org/10.1029/98JA00103

Vaisberg, O. L. (1976). Mars-plasma environment. In D. J. Williams (Ed.), *Physics of solar planetary environment* (pp. 854–871). Boulder, CO: American Geophysical Union.

Vaisberg, O. L., Ermakov, V. N., Shuvalov, S. D., Zelenyi, L. M., Znobishchev, A. S., & Dubinin, E. M. (2017). Analysis of dayside magnetosphere of Mars: High mass loading case as observed on MAVEN spacecraft. *Planetary and Space Science*, *147*, 28–37. https://doi.org/10.1016/j.pss.2017.09.005

Vaisberg, O. L., & Zelenyi, L. M. (1984). Formation of the plasma mantle in the Venusian magnetosphere. *Icarus*, *58*(3), 412–430. https://doi.org/10.1016/0019-1035(84)90087-3

Withers, P., Matta, M., Lester, M., Andrews, D., Edberg, N. J. T., Nilsson, H., et al. (2016). The morphology of the topside ionosphere of Mars under different solar wind conditions: Results of a multi-instrument observing campaign by Mars Express in 2010. *Planetary and Space Science*, *120*, 24–34. https://doi.org/10.1016/j.pss.2015.10.013

Zelenyi, L. M., & Vaisberg, O. L. (1985). Venusian interaction with the solar wind plasma flow as a limiting case of the cometary type interaction. In Buti (Ed.), *Advances of space plasma physics* (pp. 59–76). Trieste: World Scientific.

Zhang, T. L., Luhmann, J. G., & Russell, C. T. (1991). The magnetic barrier at Venus. *Journal of Geophysical Research*, *96*(A7), 11,145–11,153. https://doi.org/10.1029/91JA00088

Zwan, B. J., & Wolf, R. A. (1976). Depletion of solar-wind plasma near a planetary boundary. *Journal of Geophysical Research*, *81*(10), 1636–1648. https://doi.org/10.1029/JA081i010p01636